A comparative study of the electronic structures of $SrCu_2O_2$ and $PbCu_2O_2$ by density functional theory, high resolution X-ray photoemission and electron paramagnetic resonance spectroscopy†

K. G. Godinho,[a] G. W. Watson,[a] A. Walsh,[ab] A. J. H. Green,[c] D. J. Payne,[c] J. Harmer[c] and R. G. Egdell*[c]

Received 14th December 2007, Accepted 4th April 2008
First published as an Advance Article on the web 24th April 2008
DOI: 10.1039/b719364e

The electronic structures of $SrCu_2O_2$ and $PbCu_2O_2$ have been studied by density functional theory calculations in conjunction with high resolution X-ray photoemission spectroscopy (XPS) and electron paramagnetic resonance spectroscopy (EPR). In both materials there is linear O–Cu–O coordination and a band of Cu 3d states sits above a band of O 2p states, but with strong hybridisation between the two. The Pb ions in $PbCu_2O_2$ introduce new states of dominant Pb 6s atomic character below the bottom of the O 2p valence band together with states of mixed Pb 6s, O 2p and Cu 3d character at the top of the O 2p valence band. Hole states introduced by K doping in $PbCu_2O_2$ are shown to reside in anisotropic sites with clearly defined hyperfine couplings to ^{63}Cu as revealed by EPR. Broadening of the EPR signal in K-doped $SrCu_2O_2$ is associated with averaging of the g value and Cu hyperfine anisotropy due to facile hole hopping. It is concluded that replacement of Sr with Pb does not facilitate delocalisation of the holes.

Introduction

There is a growing interest in the development of electronic and optoelectronic devices based on oxides which are transparent in the visible region but which can be doped to induce a high electrical conductivity. Most of the established transparent conducting oxides (TCOs) of this sort are n-type materials.[1] This includes the prototype TCOs SnO_2, In_2O_3 and ZnO. Reproducible p-type doping of these post-transition metal oxides is far from straightforward.[2–4] However, exploitation of transparent conducting oxides in devices such as UV diodes will only become possible if suitable wide gap oxides amenable to p-type doping can be developed. In the classical n-type TCOs, the top of the valence band is composed of O 2p states and it is not surprising that it is difficult to introduce holes into these bands: in chemical terms one is attempting to oxidise oxygen. However in Cu_2O the upper valence band states are of dominant Cu 3d atomic character and introduction of holes involves oxidation of $3d^{10}$ Cu(I) to $3d^9$ Cu(II). This process is chemically tractable and Cu_2O is indeed a p-type semiconductor. However the electronic gap in Cu_2O is of the order of 2 eV, which is too small for application in TCO devices. Fortunately the bandgaps in many ternary Cu(I) oxides are much bigger than in the parent Cu_2O. This has allowed development of a new family of p-type conducting ternary Cu(I) oxides that are transparent in the visible region. The first material of this sort was $CuAlO_2$[5,6] followed later by $CuGaO_2$[7] and $CuInO_2$.[8,9] These delafossite oxides all have low energy *indirect* bandgaps.[10] This limits their potential usefulness in optoelectronic devices. By contrast the ternary oxide $SrCu_2O_2$ has a *direct* bandgap of around 3.3 eV[11,12] and a UV-emitting p–n heterojunction was recently fabricated using p-type $SrCu_2O_2$ and n-type ZnO.[13,14] A key concept in the rational design of improved p-type TCOs is that delocalisation of Cu(II) hole states by hybridisation with states of other atoms present within the structure should help improve hole mobility and reduce the tendency for hole self trapping. In this context $PbCu_2O_2$ is of particular interest as the conventional view is that the Pb(II) cations in a ternary oxide introduce Pb 6s states close to the Fermi energy into the band structure. To date however there has been little work on the electronic structure of $PbCu_2O_2$.

The tetragonal structure of $SrCu_2O_2$ belongs to the space group $I4_1/amd$ with a unit cell containing four formula units and defined by the lattice constants $a = 5.469$ Å and $c = 9.826$ Å.[12,15] The crystal structure is shown in Fig. 1a and contains planar zig-zag O–Cu–O–Cu chains running in orthogonal [100] and [010] directions, with linear coordination about Cu to give linked O–Cu–O dumbbells. The Sr ions are surrounded by distorted octahedra of oxygen ions with the two most closely bound oxygen neighbours aligned linearly along the c axis. The crystal structure of $PbCu_2O_2$ shown in Fig. 1b is monoclinic and belongs to the lower symmetry space group $C12/c1$.[16] There are again four formula units per cell and the characteristic chains with linear O–Cu–O units are also present. The main differences between the two structures arises from the presence of Pb. While the coordination around Sr is essentially a compressed octahedron in $SrCu_2O_2$, in $PbCu_2O_2$ the Pb atoms are four coordinate with respect to oxygen. All oxygen nearest neighbours are present on one side of the Pb in a see-saw arrangement to give C_{2v} coordination geometry. This type of non-centrosymmetric

[a]*School of Chemistry, University of Dublin, Trinity College, Dublin, 2, Ireland*
[b]*National Renewable Energy Laboratory, Golden, CO, 80401, USA*
[c]*Department of Chemistry, University of Oxford, Inorganic Chemistry Laboratory, South Parks Road, Oxford, UK OX1 3QR. E-mail: russell.egdell@chem.ox.ac.uk*

† Electronic supplementary information (ESI) available: X-Ray powder patterns; conductivity data; full band structures. See DOI: 10.1039/b719364e

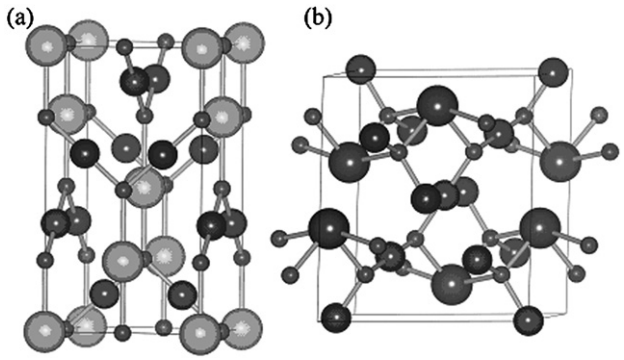

Fig. 1 The crystal structures of (a) $SrCu_2O_2$ and (b) $PbCu_2O_2$. The Sr and Pb ions are represented by large spheres, Cu ions by medium spheres and O ions by small spheres.

geometry is frequently found in Pb(II) compounds and is often attributed to onsite hybridisation between the $6s^2$ electron pair and nominally empty Pb 6p states. However we have recently shown that the stereochemical influence of the lone pair in PbO is in fact mediated by covalent interactions between anion and cation states,[17–19] and it may be anticipated that a similar situation will pertain in $PbCu_2O_2$.

In the present paper we present a comprehensive comparative study of the electronic structures of $PbCu_2O_2$ and $SrCu_2O_2$. High resolution valence band X-ray photoemission spectra are presented and compared with the results of density functional theory calculations. It emerges that occupied electronic states associated with Pb are dominantly well below the Fermi level. Moreover replacement of Sr by Pb suppresses rather than enhances hybridisation between Cu 3d and O 2p states and leads to an increase in the effective mass for the topmost valence band. This explains the disappointing finding that the tendency for hole localisation is if anything greater in $PbCu_2O_2$ than $SrCu_2O_2$. Electron paramagnetic resonance (EPR) spectroscopy is used to confirm that the hole states in doped $PbCu_2O_2$ are localised mainly on Cu, whilst in $SrCu_2O_2$ there is facile hole hopping at room temperature.

Computational

The electronic structures of $SrCu_2O_2$ and $PbCu_2O_2$ were calculated using density functional theory as implemented in VASP.[20,21] This used the gradient corrected (GGA-DFT) exchange–correlation functional parameterization scheme of Perdew, Burke and Ernzerhof.[22] The energy cutoff for the plane wave basis set and the *k*-point grid density were both rigorously checked for convergence, resulting in an upper energy threshold of 500eV. A $8 \times 8 \times 6$ Monkhorst–Pack[23] *k*-point grid was employed for $SrCu_2O_2$ with a $6 \times 6 \times 8$ grid for $PbCu_2O_2$. In addition to the inclusion of scalar relativistic effects, explicit treatment of spin–orbit coupling for the valence electrons was included. The interactions between the valence and core electrons (Cu: [Ar], Sr: [Ni], Pb: [Xe], O: [He]) were treated using the projector augmented wave method.[24] Note that our treatment includes the shallow core Sr 4s and 4p levels and the Pb 5d levels. However these levels were found not to be significantly involved in the bonding and make minimal contributions to the valence density of states. Complete optimizations of the cell angles and vectors were performed, relaxing the atomic positions so that the quantum mechanical forces were reduced to below 1 meV $Å^{-1}$.

Experimental

$SrCu_2O_2$ was prepared by firing an intimately ground and pelletised mixture of $SrCO_3$ and CuO (Sigma-Aldrich 99.99+%) at 950 °C for 72 h under flowing high purity argon with intermediate regrinding and pelletisation at 24 h intervals. This procedure represents a minor modification of a published synthesis procedure[12] with replacement of Cu_2O by CuO, because the latter can be obtained commercially with higher purity. However Cu(II)O decomposes to the Cu(I) state under the conditions employed so the two procedures are equivalent. K-doped material was prepared by a similar procedure but with replacement of a fraction x of the $SrCO_3$ with $x/2$ of K_2CO_3 to give a product with nominal composition $Sr_{1-x}K_xCu_2O_2$. $PbCu_2O_2$ was prepared by reaction between Cu_2O and PbO (Sigma-Aldrich 99.9+%) at 700 °C under flowing high purity Ar.[16,24] The product was then reground, pelletised between tungsten carbide dies and sintered for 12 h at 700 °C under flowing Ar. The Cu_2O itself was made by decomposing 99.99+% purity CuO (Sigma-Aldrich) to Cu_2O under flowing Ar at 1000 °C for 12 h. K-doped samples were prepared similarly, with some PbO being replaced by K_2CO_3 (Sigma-Aldrich 99.995+%). These samples were fired at the lower temperature of 675 °C to avoid sample melting. Phase purity for all samples was established by X-ray powder diffraction. All observed reflections in the X-ray powder patterns could be indexed on the basis of previously published lattice parameters for $SrCu_2O_2$[15] and $PbCu_2O_2$.[16] The $SrCu_2O_2$ pellets used for XPS studies had predominant (110) texture, whilst $PbCu_2O_2$ showed pronounced (103) texture. XRD line broadening suggested a grain size of order 90 nm for $SrCu_2O_2$ and 50 nm for $SrCu_2O_2$. Electrical conductivities were measured using a four probe technique. Rectangular bars were cut from the ceramic pellets using a diamond saw and mounted onto 8 pin integrated circuit holders. Contacts were attached using silver loaded epoxy resin and the relevant dimensions (bar thicknesses and distances between contacts) were determined using vernier callipers. Conductivity measurements were carried out over a range from room temperature down to at least 250 K, except in the case of undoped $PbCu_2O_2$ where the high resistivity restricted the lowest temperature to 280 K. From the slope of plots of $\log_e$(conductivity) against $1/T$, the activation energy in nominally undoped $SrCu_2O_2$ was determined to be 0.24 eV, decreasing to 0.17 eV with 2% K-doping and 0.12 eV at 5% K-doping. For $PbCu_2O_2$ higher values of 0.72 eV and 0.25 eV were observed for nominally undoped and 2% K-doped samples respectively. X-Ray powder patterns and conductivity data are given as ESI.†

High-resolution X-ray photoemission spectra were measured in a Scienta ESCA 300 spectrometer. This incorporates a rotating anode Al Kα ($h\nu$ = 1486.6 eV) X-ray source, a 7 crystal X-ray monochromator and a 300 mm mean radius spherical sector electron energy analyser with parallel electron detection system. The X-ray source was run with 200 mA emission current and 14 kV anode bias, whilst the analyser operated at 150 eV pass energy with 0.8 mm slits. Gaussian convolution of the analyser

resolution with a linewidth of 260 meV for the X-ray source gives an effective instrument resolution of 350 meV. Samples were mounted on molybdenum plates. $SrCu_2O_2$ samples were cleaned in the preparation chamber of the XPS system by rear face electron beam heating in UHV to a temperature of 700 °C for 45 min. $PbCu_2O_2$ samples were cleaned at the lower temperature of 430 °C. Binding energies were referenced to the Fermi level of a silver foil regularly used to calibrate the spectrometer. Problems with sample charging were encountered with undoped $PbCu_2O_2$ and it was necessary to stabilise surface charging with a flood gun typically operated at around 3 eV. As is usual when using a flood gun spectra were shifted to low binding energy.

X-Band EPR spectra were measured at room temperature at the EPSRC EPR National Service Centre in the Department of Chemistry, University of Manchester.

Results

Structure relaxation

Structural optimization yielded the cell parameters and bondlengths shown in Table 1. The optimized lattice vectors and bondlengths for $SrCu_2O_2$ are in very good agreement with experiment. Each of the lattice vectors are overestimated, as is expected with GGA-DFT, but they remain within 1.5% of the experimentally determined values. In the calculated equilibrium $SrCu_2O_2$ structure, the Cu ions are coordinated by two oxygen ions, at a distance of 1.86 Å. Each Sr ion is coordinated by two oxygens at 2.47 Å and four at 2.78 Å in a roughly D_{4h} environment. For $PbCu_2O_2$, while the *a* and *c* vectors are in good agreement with experiment, the *b* vector is overestimated to a more significant extent which may be attributed to the more dispersive interactions in this direction produced by the orientation of the Pb(II) lone pairs. However the Cu–O interatomic distances are correctly computed to be very similar to those in $SrCu_2O_2$. Two oxygens are closely bound to Pb at 2.31 Å, while two are further extended at 2.53 Å. This asymmetric environment is of lower symmetry than that found in litharge PbO where the four Pb–O bonds are equidistant at 4 × 2.35 Å.[17]

Electronic band structure

The calculated band structures of $PbCu_2O_2$ and $SrCu_2O_2$ close to the band edges are shown in Fig. 2. The eigenvalues are plotted along the high symmetry directions of each crystal.[25] The full band structures are included in the ESI.† For $SrCu_2O_2$ both the valence band maximum (VBM) and conduction band minimum (CBM) occur at the Γ point making it a direct gap material. The calculated Γ–Γ splitting of 1.73 eV is considerably less than the value of 3.33 eV reported experimentally. The VBM is derived from hybridized Cu 3d and O 2p orbitals, while the CBM is a mixture of Cu 4s and 3d with O 2p orbitals. The consistent underestimation of bandgaps for insulating metal oxides using DFT methods is well known, but does not effect description of ground state properties and densities of states.

Table 1 The calculated equilibrium structural parameters of $SrCu_2O_2$ and $PbCu_2O_2$. Deviations from experimental values[15,16] are given in parentheses

	$SrCu_2O_2$	$PbCu_2O_2$
Volume/Å^3	305.07	316.71
a/Å	5.559 (+1.4%)	8.285 (+0.8%)
b/Å	5.559 (+1.4%)	8.472 (+2.2%)
c/Å	9.873 (+0.5%)	6.107 (+1.5%)
β/°	90	132.37 (+0.2%)
Cu–O/Å	2 × 1.86 (+1.1%)	2 × 1.87 (+0.9%)
Sr–O/Å	2 × 2.47 (+0.4%) 4 × 2.78 (+1.4%)	—
Pb–O/Å	—	2 × 2.31 (+3.0%) 2 × 2.53 (+1.6%)

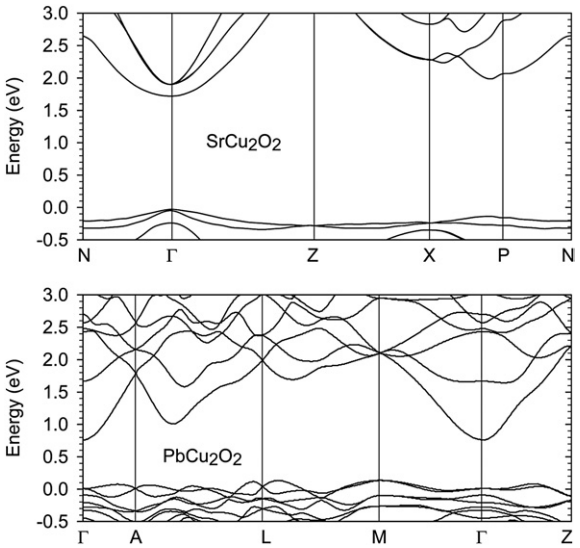

Fig. 2 The electronic band structures of $SrCu_2O_2$ and $PbCu_2O_2$ in the region of the band edges along the high symmetry directions, plotted with reference to the top of the valence band (0 eV).

The lower monoclinic symmetry of the $PbCu_2O_2$ lattice produces a more complicated band structure. Here it is striking that the VBM is elevated by 130 meV at the M point relative to Γ, making the electronic bandgap formally indirect. The calculated Γ–Γ splitting is 0.75 eV while the M–Γ splitting is 0.62 eV. Experimentally the electronic gap has been estimated at 1.7 eV from optical measurements, but there is no indication of whether the lowest energy transition is direct or indirect in nature.[26] The VBM at M is composed of hybridized Cu 3d and O 2p states, while the CBM at Γ is a mixture of Cu 4s, 3d and O 2p states but with an additional Pb 6p contribution.

We have used the dispersions in $SrCu_2O_2$ and $PbCu_2O_2$ to derive values for hole effective masses for the topmost valence bands, which originate at Γ for $SrCu_2O_2$ and at M for $PbCu_2O_2$. This was achieved by fitting a quadratic dispersion relationship to the highest valence bands along the most dispersive direction over a range of wavevectors extending from the origin to 0.02 × $2\pi/a$, where *a* is the relevant lattice parameter. For $SrCu_2O_2$ the dispersion is taken along Γ–N, whilst for $PbCu_2O_2$ the direction is M–L. In non-relativistic calculations the valence band maximum in $SrCu_2O_2$ is associated with a twofold degenerate $\Gamma_5(E_g)$ state at the Γ point. One component of this disperses more strongly to give a light hole band and the second gives a less strongly dispersing heavy hole band. The degeneracy at Γ is lifted by spin–orbit coupling which elevates the heavy hole band about 20 meV above the light hole band at Γ. The respective effective

masses are $-0.76m_0$ (heavy hole) and $-0.59m_0$ (light hole), where m_0 is the free electron mass. These values are much lower than for $PbCu_2O_2$ where we obtain $m_h = -2.3m_0$ for the topmost valence band. Note that the calculated effective masses are somewhat arbitrary and dependent upon the range of *k*-points used to fit the dispersion.

Electronic density of states

The calculated total and partial electronic density of states (EDOSs) for $SrCu_2O_2$ and $PbCu_2O_2$ are shown in Fig. 3. The atomic projections were calculated using sphere radii of 1.45 Å for Cu, 1.55 Å for Sr and Pb respectively and a radius of 1.45 Å for O. These radii were determined from consideration of the calculated valence electron density around each ion and electron counting.[27]

In the simplest ionic model description $SrCu_2O_2$ is a d^{10} Cu(I) oxide with an upper valence band of filled Cu 3d states that sits above a band of filled O 2p states. Within the linear O–Cu–O units the Cu $3d_{z^2}$ orbitals have σ-like symmetry, the $3d_{xz}$ and $3d_{yz}$ π-like symmetry and the $3d_{xy}$ and $3d_{x^2-y^2}$ δ-like symmetry. Thus O 2p orbitals can mix with Cu $3d_{z^2}$ *via* strong σ overlap and with $3d_{xz}$ and $3d_{yz}$ *via* weaker π interactions. However the $3d_{xy}$ and $3d_{x^2-y^2}$ orbitals must remain localised on Cu as there are no orbitals on oxygen of the correct δ symmetry for covalent mixing. In agreement with these qualitative ideas it is possible to identify three components within the Cu 3d bands, labelled *a*, *b* and *c* in Fig. 3. The lower non-bonding Cu 3d states in *b* and *c* exhibit very little hybridisation with O 2p states whereas the Cu 3d states in *a* at the top of the valence band have significant O 2p character. Conversely the states of dominant O 2p character are split into two bands labelled *c* and *d*. There is significant Cu 3d

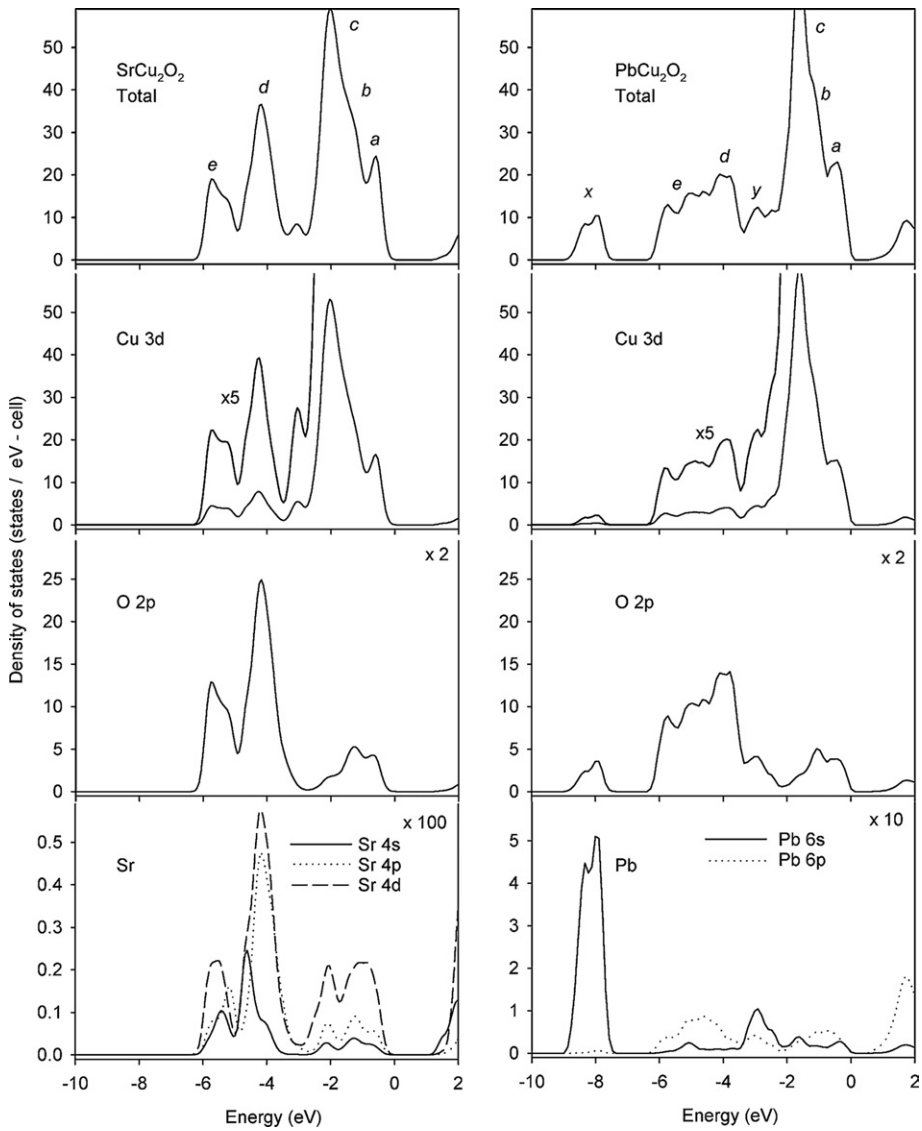

Fig. 3 Left panels: the calculated electronic density of states of $SrCu_2O_2$. From top to bottom total EDOS, Cu 3d partial EDOS, O 2p partial EDOS, Sr partial EDOS. Right panels: the calculated electronic density of states of $PbCu_2O_2$. From top to bottom total EDOS, Cu 3d partial EDOS, O 2p partial EDOS, Pb partial EDOS.

admixture into these states, mirroring the O 2p character in the Cu 3d bands *b* and *a*. The Sr makes only a very small contribution to the density of occupied valence band states although the conduction band is dominated by Sr 4d states with more minor Cu 3d, Cu 4s, Cu 4p and O 2p contributions.

For $PbCu_2O_2$ the distribution of Cu 3d states in the valence band is similar to that in $SrCu_2O_2$ and again we label three components *a*, *b* and *c*. The splitting of the bands of dominant O 2p character into two components is less well defined and there is a little less mixing of Cu 3d character into these bands than in $SrCu_2O_2$. Thus the ratio of the Cu 3d to O 2p amplitude at the peak maximum in band *d* is 0.30 for $SrCu_2O_2$ but only 0.28 for $PbCu_2O_2$. At the same time there is more pronounced mixing of counter cation states (in this case Pb 6p) into the O 2p bands than is apparent for $SrCu_2O_2$. Finally the Pb 6s states produce a new band labelled *x* in Fig. 3. This lies well below the bottom of the main O 2p valence band. There is however some mixing between the 6s states and the O 2p states, introducing bonding O 2p character into the states of band *x*. The corresponding antibonding states are found in a further band *y* which lies between the main O 2p valence bands and the Cu 3d states. For this reason the Pb 6s partial density of states has a significant contribution about 2.5 eV below the VBM. Only a little Pb 6s character is found at the top of the valence band. This situation contrasts with that in the binary oxide PbO. Here the Pb 6s states located at the bottom of the valence band again interact with O 2p states, but the filled antibonding O 2p–Pb 6s states lie at the top of the valence band.[17–19]

A number of band structure calculations for $SrCu_2O_2$ have been published previously,[12,28–33] but most have neglected spin–orbit coupling. We are unaware of any other published first-principles calculations on $PbCu_2O_2$. The calculations on $SrCu_2O_2$ have employed a range of techniques including plane-wave models based on density functional theory[12,28,29,31,32] and the tight binding linearized muffin tin orbital approach.[30] Most recently Hu *et al.* have reported calculations using a hybrid-exchange DFT approach implemented within the CRYSTAL code and based on a carefully optimised atomic orbital basis sets.[33] The densities of states from these calculations are generally in broad agreement with the results of the present work, except in the case of the recent plane-wave calculation of Modreanu *et al.*,[32] where the Sr 4d and Sr 4p contribution to the density of states within the O 2p part of the valence band appear to have around 25% of the amplitude of the corresponding Cu 3d contribution. In the other calculations, including our own, the contribution is around 5%. However the sphere radii used in the projection of partial densities of states is not specified in this study. A critical comparison between the current calculation and the hybrid Hamiltonian calculation of Hu *et al.*[33] benchmarked against valence band XPS data is given in the next section.

X-Ray photoemission

Widescan X-ray photoelectron spectra of $SrCu_2O_2$ and $PbCu_2O_2$ after sample cleaning as described earlier are shown in Fig. 4. All the core level and Auger peaks can be assigned to Sr, Cu and O in the case of $SrCu_2O_2$ and to Pb, Cu and O in the case of $PbCu_2O_2$. In particular there is no evidence of significant C contamination, which would be signalled by the appearance of a C 1s peak at

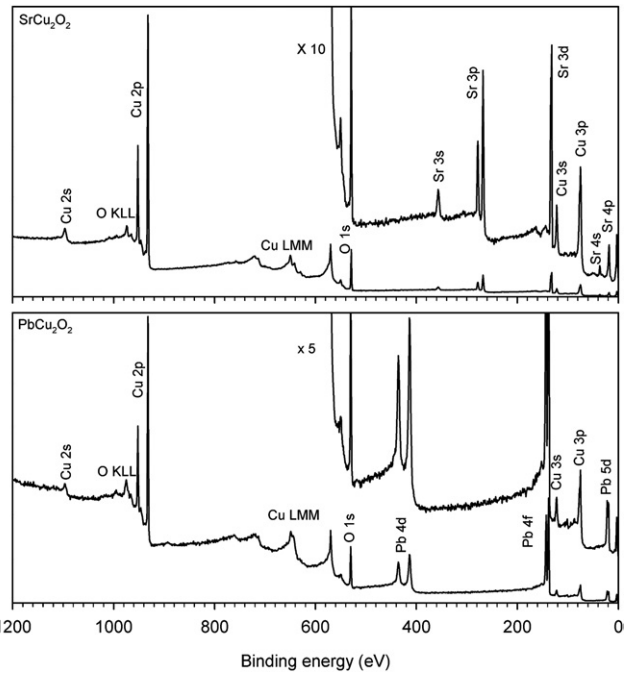

Fig. 4 Widescan XPS data for $SrCu_2O_2$ and $PbCu_2O_2$ after *in situ* sample cleaning as described in the text.

~285 eV binding energy. Narrow scan measurements on Sr 3d, Cu $2p_{3/2}$ and O1s core levels for $SrCu_2O_2$ and on Pb $4f_{7/2}$, Cu $2p_{3/2}$ and O 1s core levels for $PbCu_2O_2$ allow us to derive values for effective surface stoichiometries after correction with the relevant atomic sensitivity factors.[34] In this way we obtain $Sr_{1.03}Cu_{1.97}O_{2.09}$ and $Pb_{0.94}Cu_{2.06}O_{2.03}$. Given uncertainties on the order of 5% in atomic sensitivity factors and that the strongest core lines span a wide range of kinetic energies, these values are in excellent agreement with the nominal bulk stoichiometries.

Valence band photoemission spectra of nominally undoped $SrCu_2O_2$ and $PbCu_2O_2$ are shown in the upper panels of Fig. 5. The experimental valence band spectrum for undoped $SrCu_2O_2$ is in good agreement with a valence band spectrum published previously for a K-doped sample.[34,35] In this earlier work the main effect of K doping was found to be a downward shift in the Fermi level toward the valence band edge. Since all binding energies are referenced to the Fermi energy, doping leads to a small decrease in binding energies which correlates with the change in the activation energy for conduction.[35] For undoped $SrCu_2O_2$ the Fermi level lies 0.24 eV above the valence band edge, in agreement with experiment. To facilitate comparison between the present experimental data and the band structure calculation, the spectrum for $SrCu_2O_2$ has been arbitrarily shifted so that the zero of the binding energy scale coincides with the top of the valence band. A similar procedure was applied for $PbCu_2O_2$ where the position of the valence band edge relative to the Fermi level cannot be determined from experiment due to the influence of the flood gun.

The lower panels in Fig. 5 show the sum of partial densities of states for $SrCu_2O_2$ and $PbCu_2O_2$ with the contribution for each orbital type weighted by ionisation cross sections calculated by Yeh and Lindau.[36,37] The basis of this approach, which was first

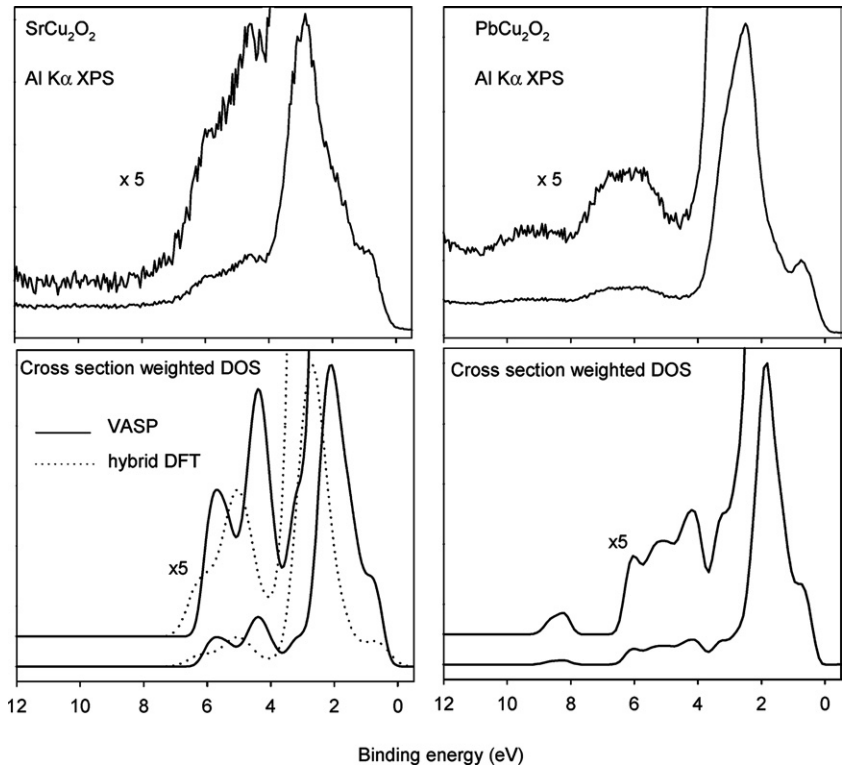

Fig. 5 Upper panels: valence band X-ray photoemission spectra of $SrCu_2O_2$ and $PbCu_2O_2$. Lower panels: cross section weighted densities of states from VASP calculations. The panel for $SrCu_2O_2$ also shows the cross section weighted density of states derived from a hybrid-DFT calculation.[33] Partial densities of states were broadened by a Gaussian with full width at half maximum height of 1 eV to account for experimental and phonon broadening of the experimental data.

proposed by Gelius *et al.* in the context of molecular ionisation cross sections,[38] is that under Al Kα excitation, the de Broglie wavelength of the final state photoelectrons deriving from valence levels is only about 0.3 Å and thus the dipole matrix elements which determine the ionisation cross sections are overwhelmingly dominated by regions of space very close to the atomic nuclei.[39] In agreement with previous work[40] comparing cross section weighted densities of states derived from VASP calculations with high resolution X-ray photoemission data there is good agreement between experiment and calculation. This is both in terms of the shape of the overall spectral profiles and the intensity of the O 2p region of the valence band relative to the Cu 3d region. At Al Kα energies the one electron cross section for ionisation of Cu 3d states (1.2×10^{-3} Mb) is a factor of 20 bigger than the cross-sections for ionisation of O 2p states (6×10^{-5} Mb), whilst the low value for the Cu 4s cross section (2.7×10^{-4} Mb) coupled with the very small contribution of Cu 4s states to the valence band means that they too make a negligible contribution to the cross section weighted density of states. The Sr contribution to the partial density of states is also very small and the Sr 5s cross section (1.5×10^{-4} Mb) is again low[41] so again these states make a negligible contribution compared to Cu 3d. For these reasons the spectrum for $SrCu_2O_2$ basically mirrors the Cu 3d partial density of states rather than the total density of states. The appearance of intensity in the region of the O 2p states therefore arises mainly from covalent mixing between Cu 3d and O 2p states. The greater peak maximum intensity of the O 2p structure in the spectrum of $SrCu_2O_2$ as compared with that in the spectrum of $PbCu_2O_2$ is therefore a direct reflection of the greater amplitude of the Cu 3d contribution in the O 2p valence band in the former, as seen in the calculations. The spectra of $PbCu_2O_2$ also show that the location of Pb 6s states below the bottom of the O 2p valence band suggested by the calculations is reproduced in experimental data with the appearance of a distinct peak corresponding to band *x* of the theoretical spectra.

It is interesting to compare (Fig. 5) the cross section weighted density of states from the present calculation with that derived from a recent calculation using a hybrid-DFT approach.[33] This calculation gives a value for the bandgap of 3.4 eV, very close to the experimental value.[12,32] However, the computed cross section weighted density of states profile differs noticeably from that derived from the GGA-DFT calculation and also differs from experiment. In particular the intensity of the leading feature *a* at the top of the valence band relative to the peak maximum *c* is about 0.31 in the VASP calculation and 0.09 using the CRYSTAL code, as compared with an experimental value of 0.26. Similarly the intensity of the peak *d* in the O 2p region relative to *c* is 0.17 in VASP and 0.10 in CRYSTAL, as compared with an experimental value of 0.17. Somewhat surprisingly then a calculation which gives a good absolute value for the bulk bandgap does a less good job in reproducing the Al Kα XPS spectral profile than the VASP approach. This is particularly noticeable in relationship to the XPS intensity in the bottom half of the valence band, which is a direct probe of the extent of Cu 3d–O 2p hybridisation.

Electron paramagnetic resonance spectra

Preliminary experiments showed that undoped cuprite samples gave rather weak EPR spectra dominated by the empty cavity signal of the EPR spectrometer. We therefore restrict our discussion to doped samples where both EPR and magnetic susceptibility measurements (not presented) showed that there was a much higher concentration of unpaired spins. X-Band EPR spectra of K-doped $SrCu_2O_2$ and $Pb_2Cu_2O_2$ are shown in Fig. 6. It was found from both EPR and magnetic susceptibility measurements that the concentration of paramagnetic hole centres was always less than the nominal K-doping level. This shows that there is significant compensation of the holes nominally introduced by K doping by some sort of n-type donor defects, possibly oxygen vacancies or cation interstitials. Moreover the degree of compensation was greater for $SrCu_2O_2$ than $PbCu_2O_2$ so that at a given K-doping level the concentration of paramagnetic centres was greater for $PbCu_2O_2$ than $SrCu_2O_2$. In order to compare spectra from samples of $SrCu_2O_2$ and $Pb_2Cu_2O_2$ with similar concentrations of paramagnetic centres it was therefore necessary to select samples with different K-doping levels. Data are presented for 2.5% K-doped $PbCu_2O_2$ where the concentration of paramagnetic centres as determined from the EPR intensity was 0.9% of copper cation sites and for 5% K-doped $SrCu_2O_2$ where the concentration had a value of 0.7%. The spectra for both samples were characteristic of Cu(II) in an axial environment. The spectrum for the K-doped $PbCu_2O_2$ could be simulated with a static spin Hamiltonian[42] with parameters $g_{\|} = 2.292$, $g_{\perp} = 2.056$ and hyperfine coupling constants $A_{\|}$ (^{63}Cu) = 450 MHz and $A_{\perp}$ (^{63}Cu) = 40 MHz. The linewidth was 100 MHz. The spectrum from $SrCu_2O_2$ was modelled with similar parameters $g_{\|} = 2.295$, $g_{\perp} = 2.060$, $A_{\|}$ (^{63}Cu) = 500 MHz, $A_{\perp}$(^{63}Cu) = 65 MHz, and linewidth = 100 MHz. However it was further necessary to introduce an isotropic correlation time of $\tau \sim 7 \times 10^{-11}$ s corresponding to a frequency of 1.4×10^{10} s^{-1}, *i.e.* 14000 MHz. This leads to spectral broadening and the onset of coalescence of the $g_{\|}$ and $g_{\perp}$ components of the spectrum. In solution g value averaging arises from molecular rotation. This is clearly not relevant to the solid state. However hopping of the paramagnetic hole centres between Cu sites in a polycrystalline material can mimic the effects of rotation in solution. Within each unit cell of the $SrCu_2O_2$ structure there are four different orientations of the O–Cu–O dumbbells so that hopping between sites within a single crystallite will lead to g value averaging further enhanced by hopping across grain boundaries between crystallites. From the difference in activation energy for hole hopping of 0.13 eV between 5% K-doped $SrCu_2O_2$ and 2% K-doped $PbCu_2O_2$ we can estimate that the hole hopping rate is a factor of about 200 greater in the doped $SrCu_2O_2$ at room temperature where $kT \sim 0.025$ eV. Thus in doped $PbCu_2O_2$ inter-site hopping corresponds to an inverse correlation time of 14000/200 MHz, *i.e.* 70 MHz. This will have minimal impact on the experimental spectrum. We can further compare the inverse correlation time of 1.4×10^{10} s^{-1} for 5% K-doped $SrCu_2O_2$ with a hopping frequency derived by multiplying a frequency factor ν by an Arrhenius term $\exp(-\Delta E/kT)$, where ΔE is the activation energy of 0.12 eV for conduction. Hole hopping is strongly coupled to Cu–O phonon modes so that we may equate ν with a phonon energy of order 0.05 eV (400 cm^{-1}) giving $\nu = 1.2 \times 10^{13}$ s^{-1}. The Arrhenius factor is estimated to be 0.008 at room temperature so $\nu\exp(-\Delta E/kT) \sim 10^{11}$ s^{-1}. This is quite close to the inverse correlation time. It must be remembered that inter-grain hops are required to produce complete g value averaging so that it is not surprising that the estimated hopping frequency is slightly greater than the inverse correlation time.

Comparisons between $SrCu_2O_2$, $PbCu_2O_2$ and Cu_2O

Both band structure calculations and the XPS data suggest that Cu–O covalency is less pronounced in $PbCu_2O_2$ than $SrCu_2O_2$.

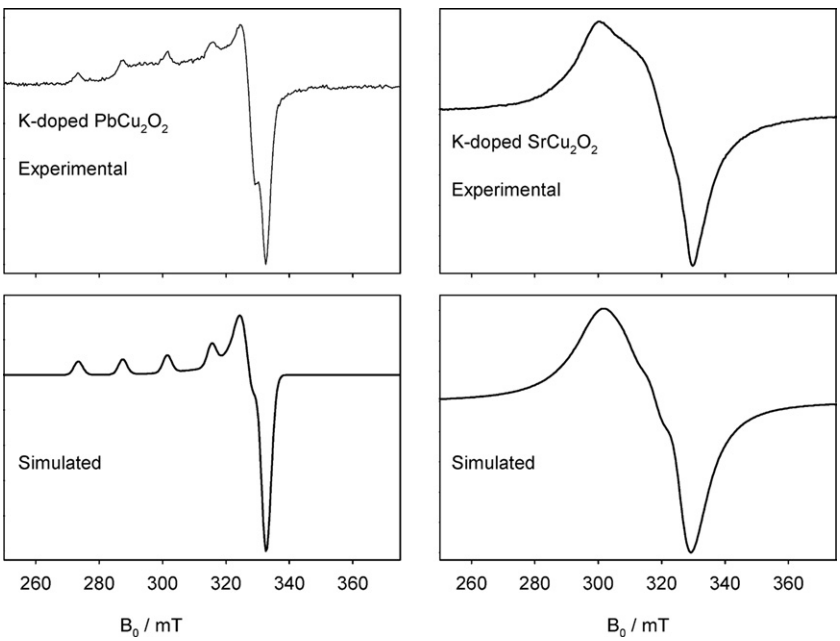

Fig. 6 Upper panels: experimental X-band EPR spectra of K-doped $PbCu_2O_2$ (9.446197 GHz) and K-doped $SrCu_2O_2$ (9.441734 GHz). The unpaired spin concentrations are respectively 0.9% and 0.7% of the Cu concentrations. Lower panels: simulated spectra using parameters discussed in text.

Table 2 Bader partial charges and experimental Cu–O bondlengths for $SrCu_2O_2$, $PbCu_2O_2$ and Cu_2O

	$SrCu_2O_2$	$PbCu_2O_2$	Cu_2O
Charge on Cu	+0.50	+0.52	+0.543
Charge on O	−1.25	−1.11	−1.086
Charge on Sr or Pb	+1.50	+1.17	—
Cu–O bondlength/Å	1.840[15]	1.862, 1.854[16]	1.849[43]

This is manifest in computed Bader partial charges[44] derived from the band structure calculations and given in Table 2. Here it may be seen that the partial charge on Cu in $PbCu_2O_2$ (+0.52) is slightly greater than in $SrCu_2O_2$ (+0.50). This difference may in turn be traced to the fact that Pb–O bonds are more covalent than Sr–O bonds so that the partial charge on Pb (+1.17) is much less than the partial charge on Sr (+1.50). At the same time the partial charge on O is $PbCu_2O_2$ (−1.11) is less than in $SrCu_2O_2$ (−1.25) due to the enhanced Pb–O covalency. These electronic differences are reflected in the fact that the experimental Cu–O bondlengths in $PbCu_2O_2$ (1.862 Å and 1.854 Å)[16] are slightly longer than the corresponding bondlength in $SrCu_2O_2$ (1.840 Å).[15] The subtle differences in Cu–O bonding in turn lead to a pronounced increase in the effective mass for the topmost valence bands between $SrCu_2O_2$ ($m^* = -0.76m_0$ and $-0.59m_0$) and and $PbCu_2O_2$ ($m^* = -2.3m_0$). In a hydrogenic model, hole binding energies at very low doping levels are proportional to the valence band effective mass. There is therefore a pleasing correspondence between the difference in effective masses of the topmost bands from the band structure calculations and the factor of 3 difference in activation energies for conduction of nominally undoped $SrCu_2O_2$ and $PbCu_2O_2$.

Finally it is possible to make some comparison between the MCu_2O_2 compounds and the parent compound Cu_2O. The primitive cubic structure of Cu_2O is based on a body centred cubic array of oxygen ions with Cu ions occupying half the sites between adjacent oxygen ions. The structure can alternatively be described in terms of two interpenetrating anti-SiO_2 cristobalite nets.[45] In this structure the Cu ions occupy sites with linear coordination by two O ions with an experimental Cu–O bondlength of 1.849 Å,[45] intermediate between the values for the two MCu_2O_2 compounds. There have been at least nine previous band structure calculations on Cu_2O (see ref. 46 and references therein), including two recent studies using the VASP code.[32,47] The computed effective mass in Cu_2O ($-0.4m_0$) is smaller than for both $SrCu_2O_2$ and $PbCu_2O_2$ and is little effected by introduction of the Cu vacancies needed to produce p-type conductivity.[32,47] Unfortunately Bader partial charges were not given in these earlier publications. We therefore repeated the VASP calculation on Cu_2O[48] and obtained partial charges on Cu and O of +0.543 and −1.086 respectively (Table 2). The partial charge on O is the lowest amongst the three Cu oxides, but the Cu partial charge is the highest. However direct comparison with $SrCu_2O_2$ and $PbCu_2O_2$ is difficult because of the absence of competing M(II) cations in Cu_2O. Perhaps the most striking difference between Cu_2O and the MCu_2O_2 species is that the computed Cu 3d bandwidth in Cu_2O is about 4.0 eV[32,47,48] which is very much greater than the values of 2.8 eV and 2.4 eV for $SrCu_2O_2$ and $PbCu_2O_2$ respectively. The different bandwidths appear to reflect the fact that in Cu_2O each Cu ion has 12 next nearest (6 within each of the two interpenetrating nets) Cu neighbours and pronounced interactions between the nominally filled $3d^{10}$ shells is therefore 3-dimensional. By contrast in $SrCu_2O_2$ and $PbCu_2O_2$ there are only two next nearest Cu neighbours and Cu–Cu interactions are confined to the 1-dimensional Cu–O–Cu–O–Cu chains.[45,46]

Concluding remarks

A comparative study of $SrCu_2O_2$ and $PbCu_2O_2$ establishes that Pb 6s orbitals make little direct contribution to electronic states at the top of the valence band in the latter material and that Pb–O covalency leads to reduced interactions between Cu 3d and O 2p states. Disappointingly it thus emerges that replacement of Sr by Pb leads to an increase rather than a decrease in activation energies for conduction. This is manifest both in terms of the measured transport properties and in the appearance of EPR spectra. Thus $PbCu_2O_2$ offers no advantages over $SrCu_2O_2$ as a potential p-type transparent conducting material.

Acknowledgements

Oxford work on transparent conducting oxides is supported by EPSRC grant GR/S94148. JH is a member of the Centre for Advanced Electron Spin Resonance (CAESR) funded under EPSRC grant EP/D408559/1. The NCESS facility is supported under EPSRC grant EP/E025722/1. KGG would like to acknowledge IRCSET for a post-graduate scholarship. TCD work is sponsored by HEA PRTLI programme, IITAC and by a SFI PI grant 06/IN.1/I92 and utilised time at the Trinity Centre for High Performance Computing. We are grateful to Dr D. Collison and Dr R. M. Kowalczyk for measurement of the EPR spectra.

References

1 *E.g.* for a discussion of n-type doping in In_2O_3 see C. G. Granqvist and A. Hultåker, *Thin Solid Films*, 2002, **411**, 1.
2 T. Yamamoto and H. K. Yoshida, *Jpn. J. Appl. Phys.*, 1999, **38**, L166.
3 M. Joseph, H. Tabata and T. Kawai, *Jpn. J. Appl. Phys.*, 1999, **38**, L1205.
4 A. Tsukazaki, H. Saito, K. Tamura, M. Ohtani, H. Koinuma, M. Sumiya, S. Fuke, T. Fukumura and M. Kawasaki, *Appl. Phys. Lett.*, 2002, **81**, 235.
5 H. Kawazoe, M. Yasukawa, H. Hyodo, M. Kurita, H. M. Yanagi and H. Hosono, *Nature*, 1997, **389**, 939.
6 H. Yanagi, S. Inoue, K. Ueda, H. Kawazoe, H. Hosono and N. Hamada, *J. Appl. Phys.*, 2000, **88**, 4159.
7 K. Ueda, T. Hase, H. Yanagi, H. Kawazoe, H. Hosono, H. Ohta, M. Orita and M. Hirano, *J. Appl. Phys.*, 2001, **89**, 1790.
8 H. Yanagi, H. Kawazoe, A. Kudo, M. Yasukawa and H. Hosono, *J. Electroceram.*, 2000, **4**, 407.
9 H. Yanagi, T. Hase, S. Ibuki, K. Ueda and H. Hosono, *Appl. Phys. Lett.*, 2001, **78**, 1583.
10 X. L. Xie, S.-H. Wei and S. B. Zhang, *Phys. Rev. Lett.*, 2002, **88**, 066405.
11 A. Kudo, H. Yanagi, H. Hosono and H. Kawazoe, *Appl. Phys. Lett.*, 1998, **73**, 220.
12 H. Ohta, M. Orita, M. Hirano, I. Yagi, K. Ueda and H. Hosono, *J. Appl. Phys.*, 2002, **91**, 3074.
13 H. Ohta, M. Orita, M. Hirano and H. Hosono, *J. Appl. Phys.*, 2001, **89**, 5720.
14 H. Hosono, H. Ohta, K. Hayashi, M. Orita and M. Hirano, *J. Cryst. Growth*, 2002, **237**, 496.

15 C. Teske and H. Muller-Buschbaum, *Z. Anorg. Allg. Chem.*, 1970, **379**, 113.
16 H. Szillat and C. L. Teske, *Z. Anorg. Allg. Chem.*, 1994, **620**, 1307.
17 A. Walsh and G. W. Watson, *J. Solid State Chem.*, 2005, **178**, 1422.
18 D. J. Payne, R. G. Egdell, A. Walsh, G. W. Watson, J. Guo, P. A. Glans, T. Learmonth and K. E. Smith, *Phys. Rev. Lett.*, 2006, **96**, 157403.
19 D. J. Payne, R. G. Egdell, D. S. L. Law, P. A. Glans, T. Learmonth, K. E. Smith, J. H. Guo, A. Walsh and G. W. Watson, *J. Mater. Chem.*, 2007, **17**, 267.
20 G. Kresse and J. Hafner, *Phys. Rev. B*, 1994, **49**, 14251.
21 G. Kresse and J. Furthmuller, *Comput. Mater. Sci.*, 1996, **6**, 15.
22 J. P. Perdew, K. Burke and M. Ernzerhof, *Phys. Rev. Lett.*, 1996, **77**, 3865.
23 H. J. Monkhorst and J. D. Pack, *Phys. Rev. B*, 1976, **13**, 5188.
24 P. E. Blochl, *Phys. Rev. B*, 1994, **50**, 17953.
25 C. J. Bradley and A. P. Cracknell, *The Mathematical Theory of Symmetry in Solids*, Clarendon, Oxford, 1972.
26 H. Yanagi, J. Tate, R. Nagarajan and A. W. Sleight, *Solid State Commun.*, 2002, **122**, 295.
27 For a fuller discussion see: A. Walsh and G. W. Watson, *Phys. Rev. B*, 2004, **70**, 235114.
28 X. L. Nie, S.-H. Wei and S. B. Zhang, *Phys. Rev. B*, 2002, **65**, 075111.
29 J. Robertson, P. W. Peacock, M. D. Towler and R. Needs, *Thin Solid Films*, 2002, **411**, 96.
30 S. Boudin, C. Felser and F. Studer, *Solid State Sci.*, 2003, **5**, 741.
31 J. Robertson, K. Xiong and S. J. Clark, *Thin Solid Films*, 2006, **496**, 1.
32 M. Modreanu, M. Nolan, S. D. Elliot, O. Durand, B. Servet, G. Garry, H. Gehan, G. Huyberechts, E. L. Papadopolou, M. Androulidaki and E. Aperathitis, *Thin Solid Films*, 2007, **515**, 8624.
33 J. P. Hu, D. J. Payne, R. G. Egdell, N. M. Harrison and V. R. Dhanak, *Chem. Phys. Lett.*, 2007, **450**, 39.
34 C. C. B. Lynch, R. G. Egdell and D. S. L. Law, *Chem. Phys. Lett.*, 2005, **401**, 223.
35 D. J. Aston, D. J. Payne, A. J. H. Green, R. G. Egdell, D. S. L. Law, J. Guo, P. A. Glans, T. Learmonth and K. E. Smith, *Phys. Rev. B*, 2005, **72**, 195115.
36 J. J. Yeh and I. Lindau, *At. Data Nucl. Data Tables*, 1985, **32**, 1.
37 The non-relativisitic Yeh and Lindau cross sections for Pb 6s and Pb 6p orbitals are incompatible with measured Al Kα valence band spectra of PbO and PbO_2. See for example ref. 18 and D. J. Payne, R. G. Egdell, G. Paolicelli, F. Offi, G. Panaccione, P. Lacovig, G. Monaco, G. Vanko, A. Walsh, G. W. Watson, J. Guo, G. Beamson, P.-A. Glans, T. Learmonth and K. E. Smith, *Phys. Rev. B*, 2007, **75**, 153102, . Semiempirical values of 6×10^{-5} Mb have been used for both orbitals.
38 U. Gelius, C. J. Allan, G. Johansson, H. Siegbahn, D. A. Allinson and K. Siegbahn, *Phys. Scr.*, 1971, **3**, 237.
39 J.-T. J. Huang and F. O. Ellison, *J. Electron Spectrosc. Relat. Phenom.*, 1974, **4**, 233.
40 P. A. Glans, T. Learmonth, K. E. Smith, J. Guo, A. Walsh, G. W. Watson, F. Terzi and R. G. Egdell, *Phys. Rev. B*, 2005, **71**, 235109.
41 Calculated cross sections for Cu 4p and Sr 5p and 4d states are not available as they are not occupied orbitals in the relevant atomic ground states. However the low cross sections for these orbitals in nearby atoms where the orbitals are occupied suggest that the cross sections must also be very low compared to Cu 3d.
42 S. Stoll and A. Schweiger, *J. Magn. Reson.*, 2006, **178**, 42.
43 X. Nie, S.-H. Wei and S. B. Zhang, *Phys. Rev. B*, 2002, **65**, 075111.
44 R. Bader, *Atoms in Molecules: A Quantum Theory*, Oxford University Press, New York, 1990.
45 A. F. Wells, *Structural Inorganic Chemistry*, Clarendon Press, Oxford, 1984.
46 J. P. Hu, D. J. Payne, R. G. Egdell, P.-A. Glans, T. Learmonth, K. E. Smith, J. Guo and N. M. Harrison, *Phys. Rev. B*, 2008, **77**, 155115.
47 M. Nolan and S. D. Elliot, *Phys. Chem. Chem. Phys.*, 2006, **8**, 5350.
48 G. W. Watson, unpublished.

